This paper is available on line at http://www.mcponline.org

Sequential Elution Interactome Analysis of the Mind Bomb 1 Ubiquitin Ligase Reveals a Novel Role in Dendritic Spine Outgrowth*[S]

Joseph Mertz‡, Haiyan Tan§, Vishwajeeth Pagala§, Bing Bai‡, Ping-Chung Chen‡, Yuxin Li‡, Ji-Hoon Cho§, Timothy Shaw§¶, Xusheng Wang§, and Junmin Peng‡§‖

The mind bomb 1 (Mib1) ubiquitin ligase is essential for controlling metazoan development by Notch signaling and possibly the Wnt pathway. It is also expressed in postmitotic neurons and regulates neuronal morphogenesis and synaptic activity by mechanisms that are largely unknown. We sought to comprehensively characterize the Mib1 interactome and study its potential function in neuron development utilizing a novel sequential elution strategy for affinity purification, in which Mib1 binding proteins were eluted under different stringency and then quantified by the isobaric labeling method. The strategy identified the Mib1 interactome with both deep coverage and the ability to distinguish high-affinity partners from low-affinity partners. A total of 817 proteins were identified during the Mib1 affinity purification, including 56 high-affinity partners and 335 low-affinity partners, whereas the remaining 426 proteins are likely copurified contaminants or extremely weak binding proteins. The analysis detected all previously known Mib1-interacting proteins and revealed a large number of novel components involved in Notch and Wnt pathways, endocytosis and vesicle transport, the ubiquitin-proteasome system, cellular morphogenesis, and synaptic activities. Immunofluorescence studies further showed colocalization of Mib1 with five selected proteins: the Usp9x (FAM) deubiquitinating enzyme, alpha-, beta-, and delta-catenins, and CDKL5. Mutations of CDKL5 are associated with early infantile epileptic encephalopathy-2 (EIEE2), a severe form of mental retardation. We found that the expression of Mib1 downregulated the protein level of CDKL5 by ubiquitination, and antagonized CDKL5 function during the formation of dendritic spines. Thus, the sequential elution strategy enables biochemical characterization of protein interactomes; and Mib1 analysis provides a comprehensive interactome for investigating its role in signaling networks and neuronal development. ***Molecular & Cellular Proteomics 14: 10.1074/mcp.M114.045898, 1898–1910, 2015.***

Mind bomb 1 (Mib1)[1], an E3 ubiquitin ligase, is a critical regulator of metazoan development with a large, and ever expanding, number of functions through interactions with a variety of protein partners. Mib1 mutants were first found in zebrafish mutagenesis screens (1), in which the mutants had neurogenic defects, most notably supernumerary primary neurons, and additional deficits in the development of somites (2), ear (3), and vasculature (4). These phenotypes are predominantly the consequences of impaired Notch signaling, as Mib1 is an essential activator of Notch Delta/Serrate/lag-2 (DSL) ligands (1). Mib1 also controls the development of several other organ and tissue systems, including gastrointestinal tract (5), limb bud (6), and the immune system (7). Mib1 is highly conserved across species. For instance, zebrafish Mib1 protein is 68%, 94%, and 94% identical to its fly, mouse, and human orthologs, respectively (8). Moreover, Mib1 has a paralog (Mib2) that shares 38% identical protein sequence with Mib1 in mouse (9). Mib2 is only abundantly expressed in adult tissue, however, and thus does not function in early development. Consistently, Mib1 knockout in mice results in embryonic mortality (10), whereas Mib2 deletion has no obvious effect on mouse development (6).

In addition to its role in cell fate determination during early development, Mib1 is also abundantly expressed in the adult brain (11) and plays an important role in neuronal morphogenesis (12). Neurons usually have two basic polarized structures, a single extended axon for sending signals and multiple branched dendrites (or more precisely, the somatodendritic compartment) for receiving signals. Many principle neurons in mammals further grow dendritic spines that are tiny protru-

From the ‡Departments of Structural Biology and Developmental Neurobiology, §St. Jude Proteomics Facility, ¶Department of Computational Biology, St. Jude Children's Research Hospital, Memphis, Tennessee 38105

Received, October 24, 2014 and in revised form, April 23, 2015

Published, MCP Papers in Press, April 30, 2015, DOI 10.1074/mcp.M114.045898

Author contributions: J.L.M., H.T., V.P., B.B., P.C., and J.P. designed research; J.L.M., H.T., V.P., and J.P. performed research; J.L.M., X.W., and J.P. contributed new reagents or analytic tools; J.L.M., Y.L., J.C., T.I.S., X.W., and J.P. analyzed data; J.L.M. and J.P. wrote the paper.

[1] The abbreviations used are: Mib1, Mind bomb 1; DSL, Delta/Serrate/lag-2; PSD, post-synaptic density; LTP, long-term potentiation; LC-MS/MS, liquid chromatography tandem mass spectrometry; AP-MS, affinity purification mass spectrometry; GST, glutathione S-transferase; TMT, tandem mass tag; FDR, false discovery rate; ppm, parts per million.

sions extended from dendritic branches, creating local postsynaptic compartments for the formation of excitatory synapses. In these synapses, the postsynaptic density (PSD) is an electron-dense membrane thickening aligned with the presynaptic active zone at synaptic junctions. During neuronal morphogenesis, axonal growth and path finding (13), dendrite formation (14), dendritic spine assembly (15), and synaptogenesis (16) are independent but highly related processes controlled by genetic elements and environmental cues. Although dramatic progress has been made in identifying the signaling cascades responsible for these processes, large gaps still remain in the connection of individual signaling components as well as in the coordination of multiple pathways. Our previous proteomics analysis identified that Mib1 is highly enriched in the PSD fraction, and regulates neurite outgrowth in postmitotic neurons (12). Mib1 conditional knockout mouse studies suggest a role in long-term potentiation (LTP) and synaptic plasticity (11), and further intriguing actions of Mib1 continue to be discovered. Mib1 was found to mediate the degradation of survival motor neuron 1 (SMN1), which contributes to spinal muscular atrophy (17). Mib1 was reported to be essential for Wnt3A activation of beta-catenin signaling through the receptor RYK (18), and a recent yeast two-hybrid screen indicated that Mib1 interacts with 81 candidate proteins beyond the canonical Notch pathway (19). The ongoing identification of new Mib1 interaction partners and functions underscores the need to characterize the Mib1 interactome *en masse* with high confidence.

The combination of affinity purification and liquid chromatography-tandem mass spectrometry (LC-MS/MS) has emerged as a powerful method for analyzing protein interaction networks. Technological advances in LC-MS/MS have continually increased the sensitivity of protein detection (20, 21), allowing for the analysis of complex samples (22). The primary advantage of this technique, however, has also proven to be its greatest weakness: without stringent washes and data filtering, a vast number of false positives are included in the resulting data sets (23). Methods such as tandem-affinity purification (24) have been developed to remove nonspecific contaminants, but two-step purification requires large quantities of starting materials and reduces sensitivity to loosely bound proteins. Removing contaminants by buffers containing high concentrations of salt and detergents can help limit false positives, but a delicate balance lies between rinsing contaminants and losing weakly bound but true interaction partners, and thus inflating false negative results. In addition, *in vivo* crosslinking and quantitative analysis are used to enhance the capture of transient interacting proteins (25, 26).

To this end, we attempted to characterize the Mib1 interactome by combining glutathione S-transferase (GST) protein affinity purification and advanced quantitative mass spectrometry. In our sequential elution strategy, Mib1 interaction partners were bound to affinity resins coated with GST-Mib1 domains, then eluted in three sequential buffers of increasing stringency. Proteins in these three eluents were identified and quantified by an isobaric labeling Tandem Mass Tag (TMT) method (15). The elution profile of each protein reflected its binding affinity to the GST-Mib1 resins. The strategy not only provides high sensitivity to recover weakly bound partners, but also allows for the affinity-based classification of the interactome and the removal of contaminants. By this approach, we were able to recover 817 putative Mib1 binding partners in adult rat brain and accepted about half of the proteins with high confidence. This study also uncovered that Mib1 interacts with CDKL5, a protein kinase implicated in early infantile epileptic encephalopathy-2 (EIEE2), a severe form of epilepsy and mental retardation in females (28). We then found that Mib1 acts to down-regulate CDKL5 and inhibits its promotion of dendritic spine outgrowth.

EXPERIMENTAL PROCEDURES

Plasmids and Antibodies—For affinity purification analysis, GST-Mib1 domains containing residues 1–401 or residues 384–801 from Mib1 were cloned onto the 3′ end of the GST tag within the pET21a bacterial expression vectors. For immunocytochemistry, Western blot analysis, and dendritic spine morphology analysis, full length and C985S point mutant Mib1 were cloned onto the 3′ ends of the HA tag in pcDNA3.1 vector and the GFP tag in peGFP vector. CDKL5 was cloned into the 3′ end of the HA tag in pcDNA3.1. The Usp9x and alpha-, beta-, and delta-catenin constructs were gifts from Drs. Y. Zheng (Johns Hopkins University) and A.P. Kowalczyk (Emory University). The antibodies used included HA rabbit polyclonal and mouse monoclonal antibodies (Abgent Inc, San Diego, CA), mouse monoclonal GFP Ab and FITC-conjugated GFP Ab (Abcam, Cambridge, MA), Streptavidin-HRP (Life Technologies, Carlsbad, CA), Usp9x, and catenin antibodies (Santa Cruz Biotechnology, Dallas, TX).

Affinity Purification and Sequential Elution—GST-Mib1 domain fusion proteins were expressed in *E. coli* and isolated by Glutathione-Sepharose resins (Amersham Biosciences/GE, Piscataway, NJ). The resins coated with GST fusion proteins were directly utilized to prepare affinity columns (1V = 1 bed volume, with 1 ml resin containing at least 1 mg of protein). Highly concentrated rat brain lysate (20V, ~10 mg/ml protein, in buffer A: 20 mM Hepes, pH 7.2, 0.1 M NaCl, 0.1% Triton X-100, 1 mM DTT, 1 mM EDTA, 1 mM EGTA, 15% glycerol, and protease inhibitors) was prepared, precleared by ultracentrifugation (~200,000 *g* for 1 h), and loaded on the columns. The columns were extensively washed with buffer A (40V, 20V per fraction), then sequentially eluted with buffer B (the same as buffer A except 0.3 M NaCl, 4V, ~0.5V per fraction), buffer C (the same as buffer A except 0.6 M NaCl and 0.5% Triton X-100, 4V, ~0.5V per fraction), buffer D (the same as buffer A except 2 M NaCl and 2% Triton X-100, 4V, ~0.5V per fraction), and finally cleaned with 2% SDS (4V). The fractions were analyzed by an SDS gel followed by silver staining.

TMT Labeling of Digested Peptides—Equal volumes of the eluents from each buffer condition were pooled to form two duplicated samples: 3 buffers × 2 replicates = 6 total samples. The samples were mixed with 5x loading buffer (20% Ficoll, 10% SDS, 50 mM Tris-HCl, pH 6.8, 0.1% bromphenol blue) and fresh DTT to 2 mM, heated at 90 °C for 5 min, and then cooled to room temperature. Fresh iodoacetamide was added to 20 mM for 15 min alkylation at room temperature in the dark. The samples were run on an SDS gel until the dye front was 3 mm past the stacking gel border to ensure complete stacking but little separation (29). After visualization via GelCode Blue

(Pierce/ThermoFisher, Waltham, MA) staining, protein bands were excised and cut into 1 mm^3 pieces for standard in-gel digestion, except that 5 mM HEPES buffer (pH 8.5) was used to replace 50 mM ammonium bicarbonate to avoid amine group reactions with TMT reagents downstream. The digested peptides were extracted from the gel pieces, dried and resuspended in 20 μl 50 mM HEPES (pH 8.5) for labeling with the 6-plex TMT labeling kit (ThermoFisher Scientific, Waltham, MA). Briefly, six peptide samples were labeled with isobaric TMT tags: TMT 126 and 129 for Low Stringency Elution (buffer B), TMT 127 and 130 for Medium Stringency Elution (buffer C), and TMT 128 and 131 for High Stringency Elution (buffer D). Labeling efficiency of each sample was verified by MS analysis. The labeling reaction was quenched by 5% hydroxylamine, pooled and dried down by SpeedVac. Finally, the sample was desalted using a Ziptip (EMD Millipore, Billerica, MA), then dried and dissolved in 5% formic acid for LC-MS/MS analysis.

Long Gradient LC-MS/MS Analysis of TMT Labeled Peptides—The analysis was based on an optimized long gradient LC-MS/MS system (30). TMT labeled peptides were loaded on a long C18 column (~1 m $\times$ 75 μm) packed with 1.9 μm resin (Dr. Amish GmbH, Germany), and eluted during a 9 h gradient (~0.15 μl/min; 20–55%; buffer A: 0.2% formic acid, 5% DMSO; buffer B: 0.2% formic acid, 5% DMSO, and 65% ACN). The column was heated to 65 °C by a butterfly portfolio heater (Phoenix S&T, Chester, PA) to reduce backpressure. The eluted peptides were analyzed on an Orbitrap Elite MS (Thermo Fisher Scientific, Waltham, MA) with one MS scan (30,000 resolution, 1×10^6 automatic gain control, and 100 ms maximal ion time) and top 10 high resolution MS/MS scans (HCD, 5×10^4 automatic gain control, 200 ms maximal ion time, 2 *m/z* isolation window, 37 normalized collision energy, and 30 s dynamic exclusion). The long gradient LC-MS/MS run was repeated once for the sample.

Acquired MS/MS raw files were converted into mzXML format and searched by Sequest algorithm (version 28 revision 13) against a composite target/decoy database (31, 32) to estimate false discovery rate (FDR). The target protein database was downloaded from the Uniprot rat database (28,863 protein entries) and the decoy protein database was generated by reversing all target protein sequences. Spectra were searched with $\pm$ 20 ppm for precursor ion and product ion mass tolerance, fully tryptic restriction, static mass shift for alkylated cysteine (+57.02146) and TMT-tagged N terminus and lysine (+229.162932), two maximal missed cleavages, and three maximal modification sites. Only *a*, *b*, and *y* ions were considered during the search. Assigned peptide spectra matches were first filtered by MS mass accuracy ($\pm$4 standard deviations, ~2 ppm, which was determined by all empirical good matches of doubly charged peptides with Xcorr at least 2.5). These good matches were also used for global mass recalibration prior to the filtering. The survived matches were grouped by precursor ion charge state and further filtered by Xcorr and ΔCn values. The cutoff values for XCorr and ΔCn were adjusted until a protein FDR lower than 1% was achieved. If one peptide was matched to multiple proteins, the peptide was represented by the protein with the highest peptide-spectrum matches (PSM) according to the rule of parsimony. Similar results were obtained using the JUMP program, a recently developed tag-based hybrid search engine (33). Raw data are available via the PRIDE database (www.proteomexchange.org, project accession: PXD001255).

Protein Quantification by TMT Labeled Peptides—Quantification of TMT labeled peptides was carried out by an in-house program in the following steps. (1) TMT reporter ion intensities of each identified PSM were extracted and recorded. (2) The raw intensities were corrected according to isotopic distribution of each labeling reagent. For instance, the TMT126 reagent produced 91.8% 126 *m/z* reporter ion, 7.9% 127 *m/z* reporter ion, and 0.3% of 128 *m/z* reporter ion. (3) The average of all six reporter ion signals was used as a reference to compute a relative intensity between each sample and the average. (4) The relative intensities of PSMs were averaged for identified proteins. (5) The average reporter ion intensities for Low, Medium, or High Stringency eluents were compared with derive the $\log_2$ ratios. (6) To analyze experimental variations, the intra-sample comparisons between technical duplicates were viewed as null experiments, showing an average standard deviation of 0.32. 5) Finally, we selected a $\log_2$ ratio cutoff of 0.8 (~2.5 fold of the null standard deviation) for comparing different samples. The eluted proteins were compared in a sequential fashion (L→M and M→H), resulting in the values of $\log_2$M/L, (Medium *versus* Low Stringency), and $\log_2$H/M, (High *versus* Medium Stringency).

Interaction Network Analysis—Enrichment of Kyoto Encyclopedia of Genes and Genomes pathways (KEGG) (34), and Gene Ontology terms was determined by analyzing the data set using DAVID Bioinformatics Resources 6.7 Functional Annotation Clustering tool (21, 22). STRING-DB (37) was used to evaluate interconnectivity between members of the pathways and processes determined to be enriched by DAVID.

Protein Preparation and Western blot Analysis—For preparation of protein extract from HEK293 cell culture, cells were rinsed, dislodged, and transferred to chilled centrifuge tubes with ice-cold PBS. Cells were centrifuged at 21,000 $\times$ *g* for 30 s at 4 °C and lysed in 1X LDS sample buffer (Life Technologies, Carlsbad, CA) with cOmplete protease inhibitor mixture (Roche Applied Science, Indianapolis, IN) and 10 mM DTT. The lysates were subsequently sonicated 6 $\times$ 3 s at 25% amplitude at 4 °C. An aliquot of the total cell lysate was used for SDS-PAGE and Western blotting.

In vitro Ubiquitination Assay—Recombinant GST-Mib1 was expressed and purified from *E. coli* as previously reported (12); and HA-CDKL5 was expressed and purified from HEK293 by immunoprecipitation with magnetic antiHA beads (Pierce/ThermoFisher, Waltham, MA). Ubiquitination was performed according to manufacturer's specifications using an *in vitro* Ubiquitinylation kit (Enzo Life Sciences, Farmingdale, NY). Briefly, HA-CDKL5-bound beads were incubated with biotinylated ubiquitin in ubiquitination buffer containing DTT and ATP, with the addition of different combinations of the UBA1 E1, the UBCH5B E2, and the GST-Mib1 E3 in a total reaction volume of 20 μl at 37 °C for 1 h. The reaction was then quenched by EDTA (5 mM) and proteins were extracted and resolved by SDS-PAGE followed by Western blot or LC-MS/MS analysis.

Primary Hippocampal Neuron Culture and Transfection—Embryonic rat brains were harvested from E21 pups, rinsed in ice-cold DPBS, and placed in ice-cold complete Hibernate E media (BrainBits LLC, Springfield, IL). Hippocampi were dissected, rinsed, and resuspended in 30 °C Papain enzymatic solution (Worthington Biochemical, Lakewood, NJ) for 5 min. The tissue was spun briefly, rinsed, and triturated using a fire-polished Pasteur pipette into Hibernate E. Finally, the cells were collected by centrifugation, resuspended in NBActiv4 (BrainBits LLC, Springfield, IL), plated at 1×10^5 cells per well on glass coverslips in 24-well plates and maintained at 37 °C and 5% CO_2. At day *in vitro* (DIV) 7, the neurons were transfected via $CaPO_4$ precipitation for morphological analysis (38), with 2 μg plasmid DNA per well, including 0.5 μg of EGFP plasmid, 0.75 μg of each experimental plasmid as indicated, and empty pcDNA3.1+ plasmid to equalize total DNA to 2 μg.

Immunocytochemistry—At DIV 14, 7 days post transfection, primary neuron cultures on glass coverslips were prepared for immunocytochemistry, confocal microscopic imaging, and subsequent morphological analysis of dendritic spines. All cells were harvested, fixed in ice-cold 4% paraformaldehyde in phosphate buffered saline (PBS) for 25 min, permeabilized with 0.05% Triton X-100 in PBS for 5 min, incubated with blocking solution (3% normal goat serum in PBS) for 40 min at room temperature, and then incubated with FITC-conju-

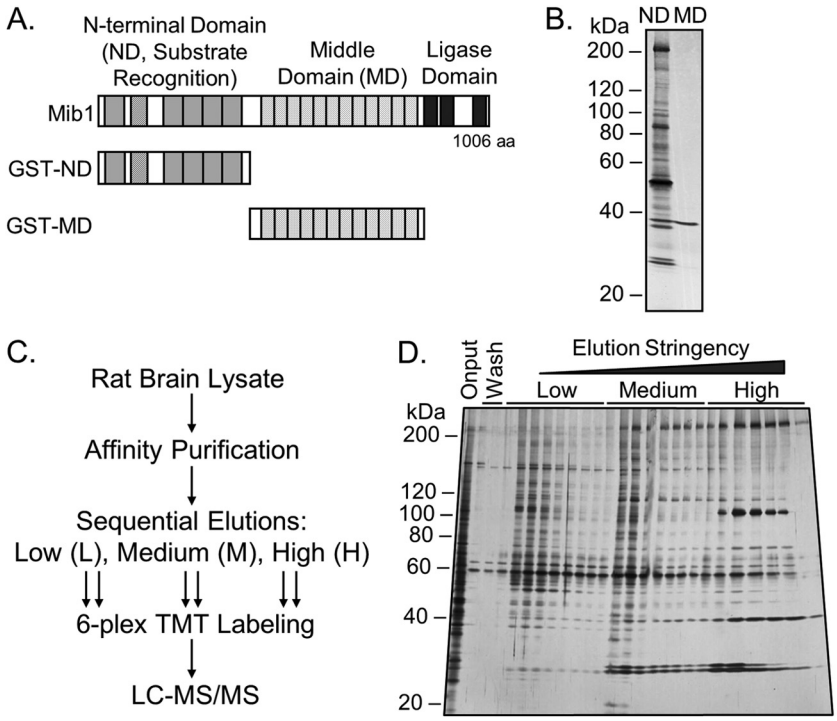

FIG. 1. **Sequential elution strategy of Mib1 affinity purification.** *A*, Domain structure of Mib1 and recombinant proteins, depicting full-length Mib1 at 1006 aa, the ND (1–401aa), and MD (384–801aa). Mib1 contains 5 Kelch repeats (gray boxes), 1 ZZ-type zinc finger domain (diagonal lined boxes), 12 ankyrin repeats (dotted boxes), and 3 RING domains (black boxes). *B*, Gel analysis of total elution from ND and MD. Total elution from ND recovered many more proteins than MD. *C*, Overview of the purification, sequential elution, TMT labeling, and LC-MS/MS strategy. Rat brain lysate was incubated with GST fusion protein beads, washed and eluted. Eluents were digested and labeled by TMT isobaric tags, mixed, and analyzed by LC-MS/MS. *D*, Sequential elution from ND. Gel analysis of sequential elutions from ND shows disparate band profiles for each buffer, including protein differences and intensities, as well as overall abundance.

gated antiGFP antibody (Abcam, Cambridge, MA) in 3% blocking solution for 1 h. The glass coverslips were washed, mounted, and sealed using ProLong Gold mounting media (Life Technologies) for confocal imaging. The transfection and staining analyses in other cells (*e.g.* HEK293) were performed by similar methods.

Dendritic Spine Morphological Analysis of Primary Hippocampal Neurons—Neurons were imaged on a Nikon (Tokyo, Japan) TE2000 C2 laser scanning confocal microscope. Images were acquired using a 60× 1.45 NA oil-immersion objective at 2048 × 2048 pixel (0.105 μm/pixel) resolution, and z-stacks were collected at 0.25 μm intervals. For analysis of dendritic spine morphology, secondary dendrites were traced manually in ImageJ (National Institutes of Health, version 1.44p 64-bit) and spines were counted and assigned into morphological categories: stubby/mushroom-shaped, thin-headed, and filopodia-like. Stubby/mushroom-shaped spines were defined as having a head width much greater than spine neck width and spine width approximately equal to spine length. Thin-headed spines exhibited a head width greater than spine neck width and spine length much greater than spine width. Filopodia-like spines were defined as those with spine length much greater than spine width and showing no prominent head. All analyses were performed in a blind manner. Totals for each category along traced lengths of dendrites were combined to calculate the overall number of spines per 10 μm for spine density analysis. Statistical significance was tested using Student's *t* test for unpaired samples and p values <0.05 were considered significant.

RESULTS

Mib1 Affinity Purification from Rat Brain and Sequential Elution—To achieve a comprehensive Mib1 interactome in the brain, we combined Glutathione S-transferase (GST) fusion protein affinity purification with quantitative mass spectrometry. The Mib1 protein can be divided into three main domains (Fig. 1*A*): the N-terminal domain that contains five kelch repeats and one ZZ zinc finger and mediates substrate binding, the middle domain composed of 12 structural ankyrin repeats, and the C-terminal domain that possesses three RING finger motifs for ubiquitin E3 ligase catalytic activity (12). Our previous small scale study showed that only the N-terminal domain binds a large number of proteins (12). We further confirmed this result in a test affinity purification analysis, in which the N-terminal domain yielded a large array of proteins, whereas the middle domain isolated only one visible band shown on a stained SDS gel (Fig. 1*B*). Thus, we determined to focus on the interactome analysis of the N-terminal domain of Mib1.

Instead of using one-step elution used in the majority of AP-MS experiments, we sequentially eluted Mib1 binding proteins with increasing buffer stringency to differentiate strong and weak binding partners from copurified contaminants (Fig. 1*C*). Nonspecific binding to either bait proteins or columns produces false positives in affinity purification experiments, and proteins that are more strongly bound—and therefore resistant to elution by buffers of low salt and detergent concentrations—are more likely to be genuine interaction partners. Despite this, simply using more stringent washes to remove weakly bound proteins without detection may result in a misleading number of false negatives. To solve this issue, we designed three sequential elution steps and analyzed all eluted proteins quantitatively by mass spectrometry, which allowed the evaluation of protein binding affinity. As visualized in the gel image (Fig. 1*D*), distinct subsets of proteins, both in identity and abundance, were eluted in the Low and Medium stringency buffers, and a remaining few proteins were recovered primarily in the final elution by the High stringency buffer. Moreover, protein patterns in all three eluents were vastly

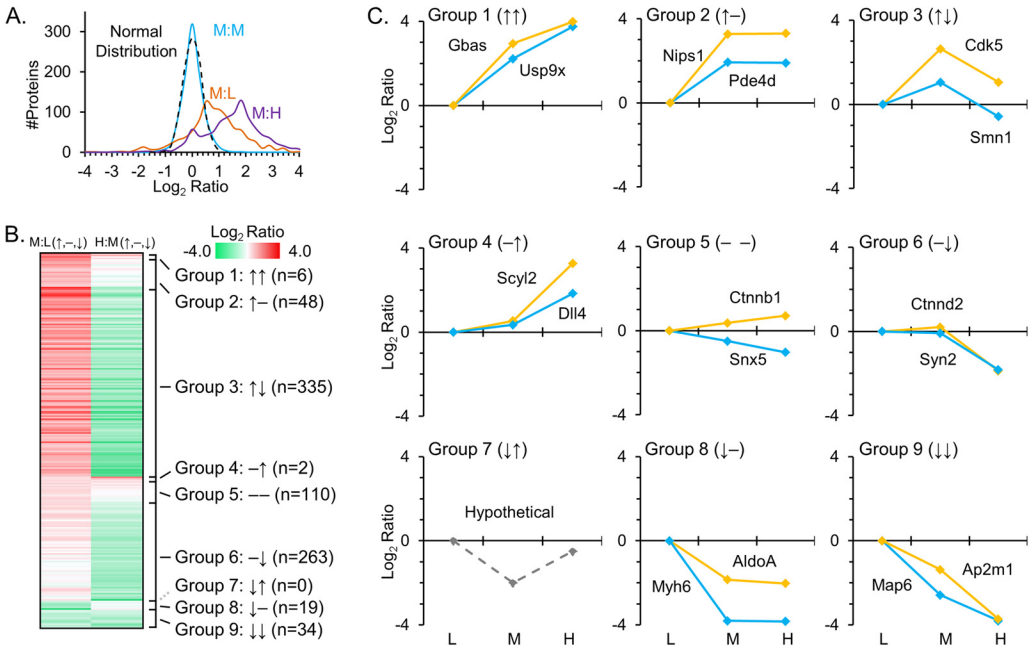

FIG. 2. **Grouping proteins by their sequential elution profiles.** *A*, Intra-elution null comparison and inter-elution experimental comparisons. Null comparison of protein abundances from Medium stringency buffer technical replicates shows a tight distribution around a $\log_2$ value of zero approaching a normal distribution. Meanwhile experimental comparisons between Medium and Low stringency buffers and between Medium and High stringency buffers display widely varied distributions, shifted toward positive values suggesting increased overall abundances in the Medium stringency elution. *B*, Heat map showing $\log_2$ values for each protein from Low to Medium elutions and Medium to High elutions. Using a log2 value of 0.8 as a threshold, proteins exhibiting increases, decreases, and no change from the Low stringency elution to the Medium stringency elution as well as Medium to High were determined. *C*, Detailed elution profiles of representative proteins from each group.

different from that in the onput (*i.e.* rat brain lysate), indicating the enrichment of a subset of proteins by the Mib1 N-terminal domain.

Sequential Elution Profiling of Mib1 Affinity-Purified Proteins by Isobaric Labeling—We then profiled the Low, Medium, and High stringency eluents by the 6-plex isobaric TMT strategy with replicates. The six samples were matched by equal volumes rather than protein amounts, allowing comparison of relative protein abundances eluted in each fraction. Briefly, the six samples were run on a short SDS gel to remove detergents and salt, followed by in gel digestion that was modified to remove all amine-reactive buffers. The resulting peptides were fully labeled by TMT reagents, pooled and analyzed twice on long gradient LC-MS/MS (~1 m x 75 μm, 9 h gradient). After database search, a total of 817 unique proteins were identified with a false discovery rate of ~1%, and their protein abundances were further obtained by the corresponding TMT tag-derived reporter ions. Nearly all proteins show variable levels among the three elution conditions (supplemental Table S1).

Global histogram analysis of the three conditions also indicated large differences (Fig. 2*A*). For example, the intra-group replicate comparison (*e.g.* M:M) of $\log_2$ ratios displayed a normal distribution centered at zero. In contrast, the inter-group comparisons (*e.g.* M:L or M:H) had small overlap with the M:M comparison, reflecting large differences in protein composition of the three samples. To assess the experimental variations, we treated the intra-group comparisons as null experiments and found that the averaged standard deviation (S.D.) of $\log_2$-ratios was 0.32. We then selected a $\log_2$-ratio cutoff of 0.8 (*i.e.* 2.5-fold of the null S.D.) that was outside a 99% confidence interval from the mean of the normal distribution. The eluted proteins were compared in a sequential fashion (L→M and M→H). As each interelution comparison resulted three possibilities: up, no change, and down, we delineated nine *elution group profiles* in the two comparisons (M:L and H:M, Fig. 2*B*).

Proteins in group 1 (n = 6) and group 4 (n = 2) were primarily eluted by the High stringency buffer (Fig. 2*C*), indicating that these proteins were firmly bound to the column and had the highest likelihood of interaction. Because of the stringency of the sequential elution profiling, only eight proteins (1% of identified proteins) were classified into these two groups, including Dll4, a Notch ligand previously known to interact with Mib1 (10); Scyl2, an endocytotic protein that induces internalization of the Wnt receptor Fzd5 (39); Gbas, a possible regulator of vesicular transport (40); and Usp9x, a deubiquitinating enzyme that stabilizes Smn1 (41) and functions in neuron migration and axon growth (42).

Proteins in group 2 (n = 48) were recovered equally by the Medium and High stringency buffers, whereas proteins in group 3 (n = 335) were eluted predominantly by the Medium

stringency buffer, showing slightly weaker affinity than those in group 2. Group 2 includes Nips1, a paralog of Gbas (also termed Nips2), Pde4d, an enzyme that mediates memory through cAMP degradation (43) and Syngap1, a major component of the PSD involved in dendritic spine formation (44). Group 3 includes Cdk5, a regulator of Mib1 level and neuronal morphogenesis; and Smn1 (41), an mRNA processing protein contributing to spinal muscle atrophy (Fig. 2*C*).

Proteins in group 5 ($n = 110$) were eluted at almost equal levels by all three buffers, whereas proteins in group 6 ($n = 263$) eluted at similar levels in the Low and Medium stringency buffer but decreased significantly in the High stringency elution. Groups 8 ($n = 19$) and 9 ($n = 34$) components were eluted largely by the first, Low stringency buffer. Collectively, these proteins are unlikely to be direct interaction partners, and the majority was simply background contaminants that would be false positives if all purified proteins were eluted together by a single buffer. Nonetheless, some proteins in these four groups might exhibit functional, but very weak affinity to Mib1, or bind Mib1 indirectly through strongly bound partners. For example, Snx5 in group 5 colocalizes with the zebrafish ortholog mind bomb in early endosomal compartments. Another group 5 protein, Beta-catenin (*i.e.* Ctnnb1), is a component of the Wnt pathway. Group 6 includes Ctnnd2, another member of the catenin family, and Synapsin II, which associates with synaptic vesicles. Group 8 contains Notch signaling component Numb1; and group 9 contains Ap2m1, which is a component of clathrin-mediated endocytosis.

Theoretically, proteins in group 7 ($n = 0$) would have been bound very weakly to be eluted by the Low stringency buffer, resistant to the Medium stringency buffer, and then also eluted at high levels by the High stringency buffer. This is unlikely, if not impossible in theory. Consistently, we found that no proteins fit this theoretical profile, which supports our assumption that proteins would elute reliably based on buffer salt and detergent concentrations in our sequential elution strategy.

In summary, the affinity of Mib1-interacting candidates can be estimated from the above eight possible elution profiles: group $4 > 1 > 2 > 3 > 5 > 6 > 8 > 9$ (Fig. 2*C*). Groups 4, 1, and 2 were accepted as high affinity binding partners, group 3 were assigned as low affinity binding partners, and the remaining four groups were likely false positives (*e.g.* copurified background proteins) or extremely weak binding proteins. Therefore, we accepted proteins identified in group 1–4 as candidates in the Mib1 interactome for subsequent studies.

To better understand Mib1 function in the brain, pathway and molecular function analysis by DAVID functional analysis software (35) revealed that Mib1-interacting proteins participate in a wide variety of biological processes: KEGG pathways (34) enriched included Spliceosome ($p < 0.001$), RNA degradation ($p < 0.001$), Gap junction ($p = 0.02$), LTP ($p = 0.03$), Neurotrophin signaling ($p = 0.05$), and Adherens junction ($p = 0.05$, supplemental Table S2) . GO terms enriched in Groups 1 through 4 included several related to RNA processing, chromatin assembly, cellular respiration, cellular morphogenesis and development, cell migration, cell adhesion, synaptic transmission and plasticity, and protein catabolism processes. We emphasized 5 key processes enriched in the Mib1 interactome, divided by groups 1 to 4 that showed relative binding affinity to Mib1 (Fig. 3), including Notch and Wnt pathways, endocytosis and vesicle transport, ubiquitin-proteasome system, morphogenesis, and synaptic activities. Further elaboration of these pathways using STRING-DB and including members of groups 5 to 9 shows high degrees of interconnectivity (Fig. 4, supplemental Fig. S1–S4), and possible means of indirect binding for many group 5 to 9 members.

Mib1 Interacts with Usp9x and Catenin Family Members—One of the most strongly bound and highly abundant proteins in our proteomics analysis, Usp9x, is a deubiquitinating enzyme that regulates embryonic development (45). The data set also included several members of the Catenin family, which participate in the Wnt signaling pathway and regulate cell adhesion (46). We analyzed these interactions with Mib1 via immunocytochemistry. When recombinant Mib1 was expressed in HEK293 cells, Mib1 colocalized almost entirely with endogenous Usp9x in puncta throughout the cytoplasm (Fig. 5*A*–5*C*). When Mib1 was co-expressed with alpha-catenin (a member of group 3), the two proteins also colocalized strongly throughout the cytoplasm (Fig. 5*D*–5*F*). Interestingly, Mib1 staining pattern was drastically altered (comparing Fig. 5*A*–5*D*), showing the dispersal of Mib1 from puncta. Similar results were obtained with beta-catenin (in group 5) and delta-catenin (*i.e.* p120, also in group 3, Fig. 5*G*–5*L*), but beta-catenin appeared to have less influence on the Mib1 staining pattern (comparing Fig. 5*A*–5*G*). The apparent distinction in the strength of Mib1 pattern alterations seen in conjunction with alpha- and delta-catenin expression *versus* beta-catenin expression may be because of the strength of their interaction, as suggested by our sequential elution strategy: alpha- and delta-catenin in group 3 have higher Mib1 affinity than beta-catenin in group 5.

Mib1 Ubiquitinates CDKL5 and Alters Its Localization, Abundance, and Functional Effects on Neuron Morphogenesis—Our Mib1 interactome analysis also revealed CDKL5 in group 3 (Fig. 6*A*), which is known to regulate neuronal morphogenesis (47) and its genetic mutations cause early infantile epileptic encephalopathy-2, a severe form of mental retardation with defects in neurodevelopment (48). When expressed in HEK293 cells, CDKL5 exhibited primarily nuclear localization (Fig. 6*B*, 6*C*). In contrast, simultaneous expression of Mib1 caused a drastic shift of CDKL5 out of the nucleus toward large cytoplasmic puncta, where the two proteins colocalized strongly (Fig. 6*D*–6*F*). Moreover, Mib1 coexpression also led to strong down-regulation of CDKL5 in a dose-dependent manner (Fig. 6*G*). This down-regulation was abol-

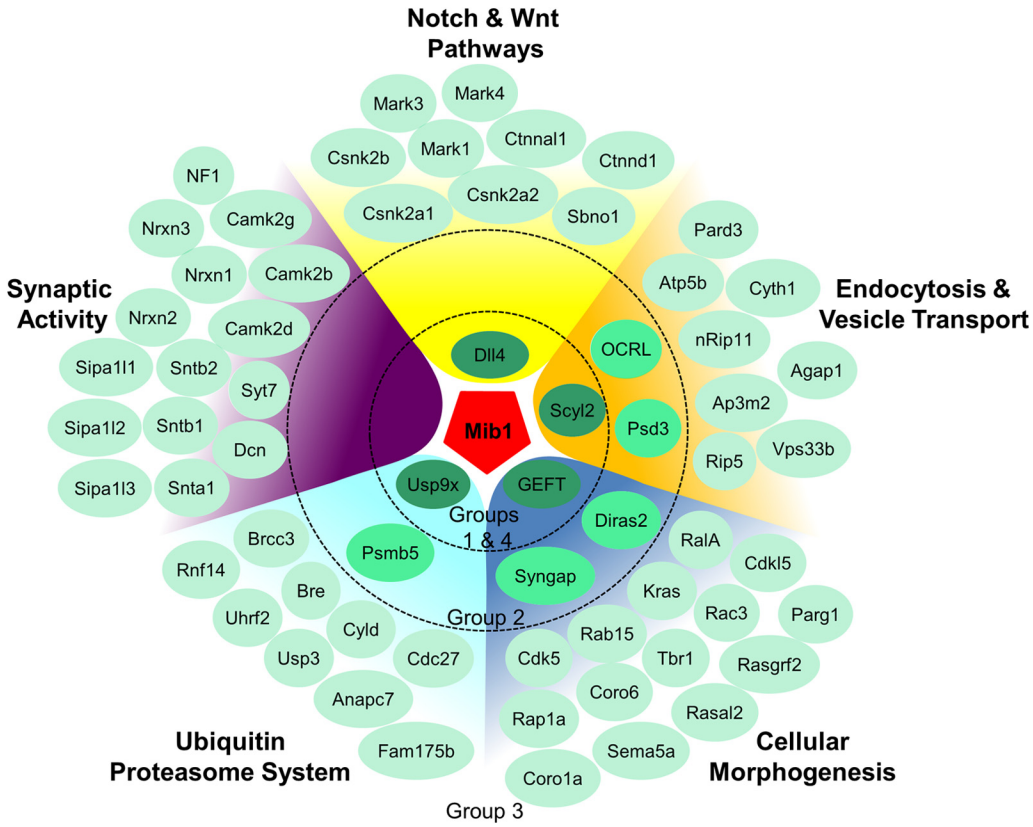

FIG. 3. **Mib1 interaction partners participate in several important signaling pathways.** Highlight of several important pathways and biological functions enriched in groups 1 through 4 in our data set. Notch signaling showed a modest enrichment, with an isoform of canonical Mib1 interaction partner delta, DLL4, exhibiting strong binding affinity and appearing in group 4. The Wnt pathway, however, was strongly enriched, with several Catenin and Casein kinase family members appearing in group 3. Proteins involved in Endocytosis and Vesicle Transport and Morphogenesis were very strongly enriched across all four elution profile groups, with clathrin-mediated endocytosis regulator Scyl2 and RhoA interaction partner GEFT showing highest affinity binding. The Ubiquitin Proteasome System was also highly enriched across elution profile groups and the Usp9x deubiquitinase displayed one of the strongest elution profiles in addition to high abundance in our analysis. Although many proteins located at Synapses and regulating LTP were recovered in our analysis, none exhibited extremely high binding affinity.

ished, and indeed may have been reversed by a point mutation (C985S) that renders the Mib1 ligase domain inactive (12) (Fig. 6*H*). These data suggest that the Mib1 ligase activity is required for the induced change in CDKL5 abundance, likely through ubiquitination and proteasomal degradation. Equal loading was determined by Ponceau S staining of membranes (supplemental supplemental Fig. S5). We also tested if Mib1 can directly ubiquitinate CDKL5 by *in vitro* ubiquitination assay. Recombinant CDKL5 and Mib1, mixed with E1, E2 enzymes, and Ub, formed a distinct Ub-positive smear with molecular size larger than CDKL5 (110 kDa). Without the addition of either E1/E2 enzymes or the Mib1 ligase, no Ub-positive smear was detected. MS analysis of the smear indicated the ubiquitination of CDKL5, and self-modification of Mib1 and E1 enzymes (Fig. 6*I*). In addition, a slight increase in the CDKL5 level was observed with the overexpression of the Mib1 C985S mutant (Fig. 6*H*), suggesting a potential dominant negative effect of C985S. Following this clue, affinity pull-down and immunocytochemical analysis showed that Mib1 binds to and colocalizes with its own C-terminal domain (Fig. 6*J*–6*K*). Therefore, Mib1 may self-associate via this domain and over-expressed C985S may form a complex with endogenous Mib1 to disrupt its activity. The data provide additional evidence for the down-regulation of CDKL5 by Mib1.

We further tested functional interaction of Mib1 and CDKL5 during neuronal morphogenesis (Fig. 7). The two proteins were reported to have opposing effects on neurite outgrowth (12, 49). The literature is somewhat conflicting in regards to the effects of CDKL5 on overall dendritic spine density - Ricciardi *et al.* reported that shRNA knockdown of CDKL5 results in increased dendritic spine density (50), whereas Zhu *et al.* reported the opposite effect of RNAi knockdown of CDKL5 (51). However, both groups agree that CDKL5 promotes dendritic spine maturation in terms of spine shape. The function of Mib1 has not been examined in this developmental process. When individually expressed in cultured hippocampal neurons, Mib1 decreased spine density by 1.19 spines/10 μm *versus* negative control ($p = 0.046$), whereas CDKL5 caused an increase of 1.43 spines/10 μm ($p = 0.049$). When

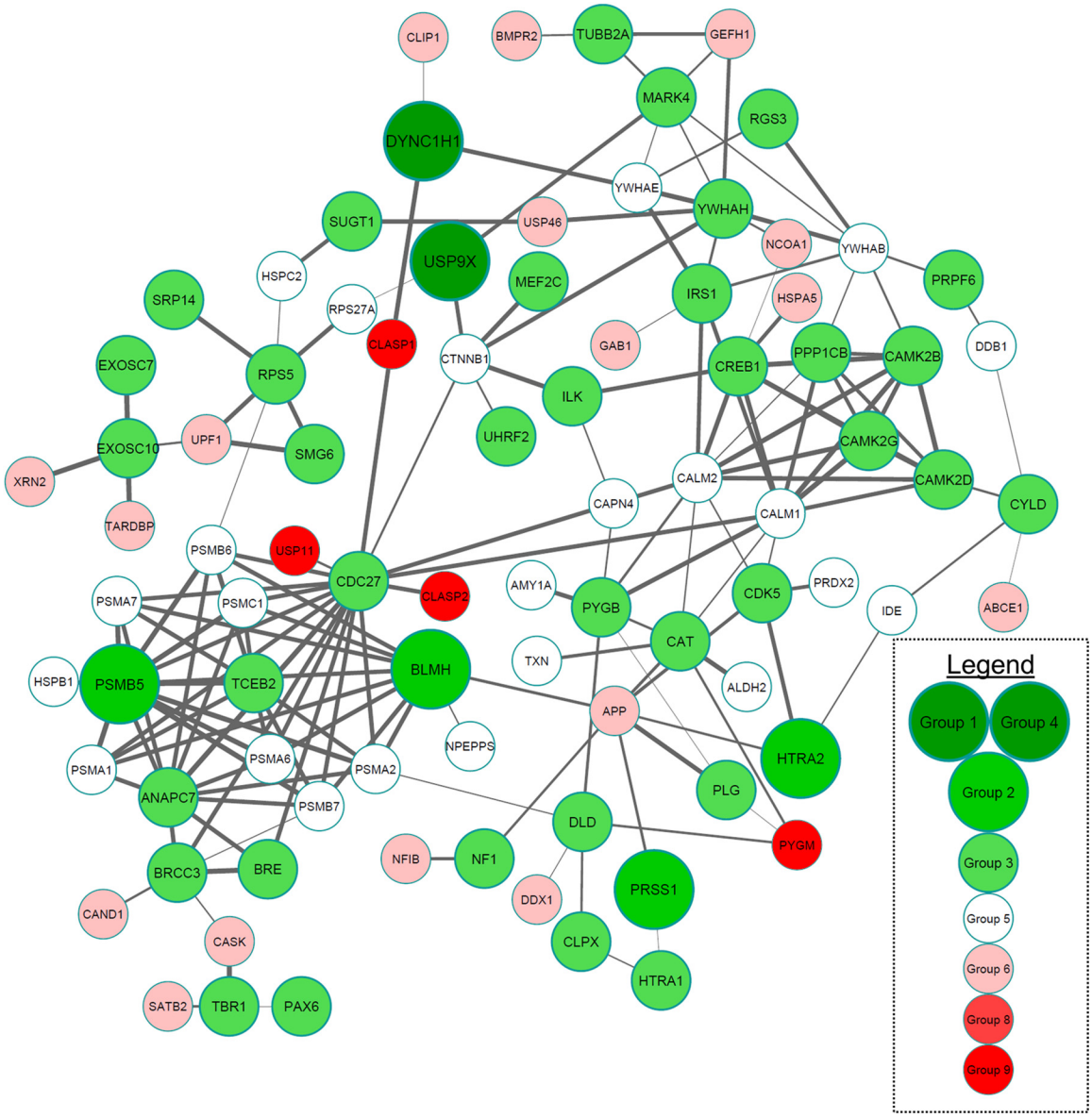

FIG. 4. **Interconnectivity in Mib1 Ubiquitin Proteasome System interactome.** Potential Mib1 interaction partners in the UPS pathway show high levels of interconnectivity. Several constituents of the Proteasome itself are included, with Proteasome Subunit Beta 5 showing highest affinity. The deubiquitinating enzyme USP9x is shown to interact with several proteins of interest as well. Edge thickness represents "combined score" from STRING-DB analysis.

co-expressed, the spine-promoting effect of CDKL5 was eliminated. These neurons exhibited 0.68 fewer spines per 10 μm than control neurons ($p = 0.252$), and far fewer (2.11/10 μm) than CDKL5 alone ($p = 0.0004$) (Fig. 7*F*). Moreover, the effects of Mib1 alone and on CDKL5 are abolished by the C985S point mutation, suggesting that the role of Mib1 is dependent on its ligase activity (Fig. 7*G*). Moreover, CDKL5 itself caused stark changes in spine morphology, shifting strongly away from immature filopodia ($p = 0.004$) toward more mature thin-headed and stubby/mushroom shaped spines ($p = 0.002$). Mib1 caused no significant effect on spine shape when compared with control, though it did limit the effect of CDKL5 when overexpressed: Mib1/CDKL5 coexpressing neurons showed a minor shift away from filopodia and thin-headed shaped spines toward stubby/mushroom shape - the effect barely reached statistical significance for the proportion of stubby/mushroom spines when compared with control ($p = 0.046$). Statistical significance was not reached for the coexpressing neurons compared with neurons expressing only Mib1 ($p = 0.614$, 0.129, and 0.104, respectively) or CDKL5 alone ($p = 0.092$, 0.297, and 0.448, respectively) (Fig. 7*H*). Together, our results also suggest that elevated CDKL5 increases spine width and maturity, and our data are consistent with the paper of Zhu *et al.* in regards to

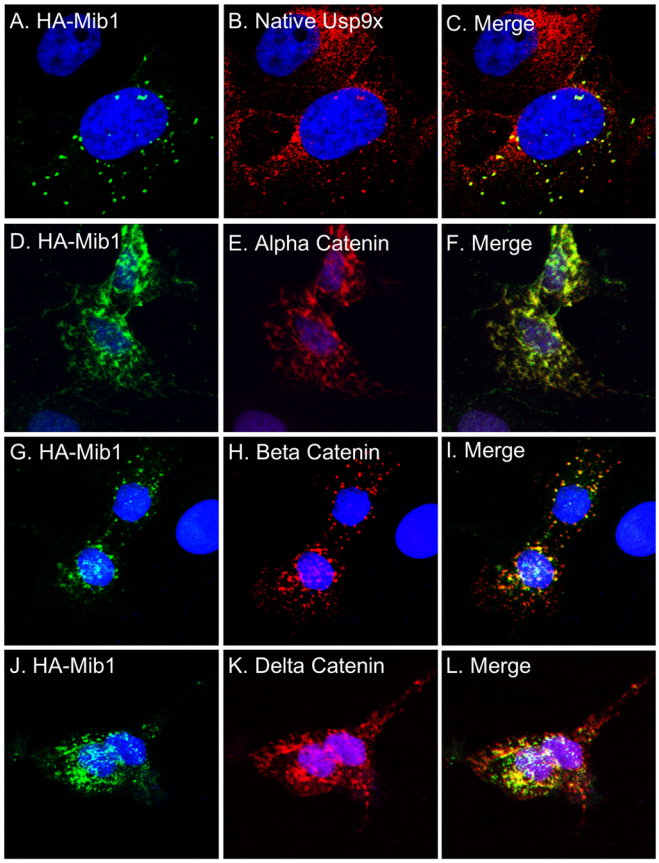

FIG. 5. **Mib1 colocalizes with Usp9x (FAM) and 3 members of the catenin family.** HEK 293 cells were transfected with HA tagged Mib1, and/or other catenin proteins, followed by immunofluorescence staining. *A–C*, Immunostaining of recombinant Mib1 and native Usp9x. *D–L*, Coexpression of HA-Mib1 and different catenin family members and subsequent immunostaining.

overall spine density. Importantly, we found that Mib1 interacts with and down-regulates CDKL5, and thus restricts the effects of CDKL5 on dendritic development.

DISCUSSION

Affinity purification coupled with mass spectrometry is a common and robust method for mining protein–protein interaction networks. The basic technique has evolved (24) and been elaborated upon (52) because its inception well over a decade ago (53), but important drawbacks remain. The challenge of nonspecific binding partners is significant. With technological advances in LC-MS/MS that improve sensitivity, the detected level of nonspecific background increases as well. The method we employed is based on a well-established concept that proteins can be eluted sequentially by buffers of increasing stringency. To our knowledge, the sequential elution strategy has not, however, been used to evaluate binding partners in a quantitative manner. Using this strategy, our data set of 817 proteins was pared down to a small subset of 56 extremely high confidence and 335 high confidence interaction partners, whereas lower confidence potential interaction partners and possible indirect binding partners were also recovered in the remaining list. Purifying and detecting large arrays of potential binding partners and distinguishing them by binding strength rather than reproducibility during biological replicates is particularly suitable for detecting low-copy number interaction partners—an ongoing technical frontier in the proteomics field (54).

We have expanded the Mib1 signaling network in breadth and functional importance. Its critical regulation of Notch-Delta signaling alone incorporates it into almost every aspect of nervous system development (6, 10, 55–60). More recently, an interactome study revealed that it also plays a role in the equally vital Wnt signaling pathway (18). Furthermore, several other potent developmental modulators beyond these key pathways have also been revealed to interact with Mib1, such as SMN1 (17) and the CDK5/p35 complex (12). In our previous study (12), Choe *et al.* presented evidence for Mib1 interaction with several other kinases in addition to proteins involved in membrane trafficking, the UPS, the cytoskeleton, and cell adhesion. These categories of Mib1 protein interaction were reiterated and elaborated upon by a yeast two-hybrid screen, revealing 81 putative binding partners for Mib1 and Mib2 (19). The present study reports an even larger list of potential Mib1 binding partners from adult rat brain, further expanding the Mib1 interaction network, reinforcing several pathways mentioned above, and introducing more components. As expected, the UPS, notch pathway, morphogenesis/cytoskeleton regulation, and endocytosis/vesicle transport pathways were strongly enriched in this data set. One somewhat unexpected result is the number of Wnt pathway members that may interact with Mib1. As mentioned previously, Mib1 had been shown to interact with one Wnt pathway member, RYK (18). Our study enlarged on this, producing a range of powerful Wnt pathway interaction partners that includes several members of the Catenin family (alpha, beta, delta1, and delta2), several MAP/microtubule affinity-regulating kinases (Mark1, 3, and 4), and Casein kinase family members.

A potential linking factor between the role of Mib1 in both Notch signaling (its canonical role), and Wnt signaling is the endocytic pathway. It is well established that Mib1 plays a critical role in Notch signaling via DSL ligand ubiquitination and endocytosis, though this molecular mechanism is still not completely clear. What is known about the process is that it is clathrin mediated, requires actin and epsin adaptors, and it may generate a mechanical pulling force on the juxtaposed Notch extracellular domain to activate signaling (61). Meanwhile, the Wnt pathway also requires clathrin mediated receptor endocytosis for successful signaling (62). Among the most highly abundant and strongest elution profiles in our data set, Scyl2 (aka CVAK104) is a relatively unstudied clathrin coated vesicle-associated kinase that binds with both the Wnt ligand receptor Frizzled 5 and the Wnt scaffold protein Dishevelled (39). This may be a common effector for Mib1 activity in these pathways, and warrants further investigation.

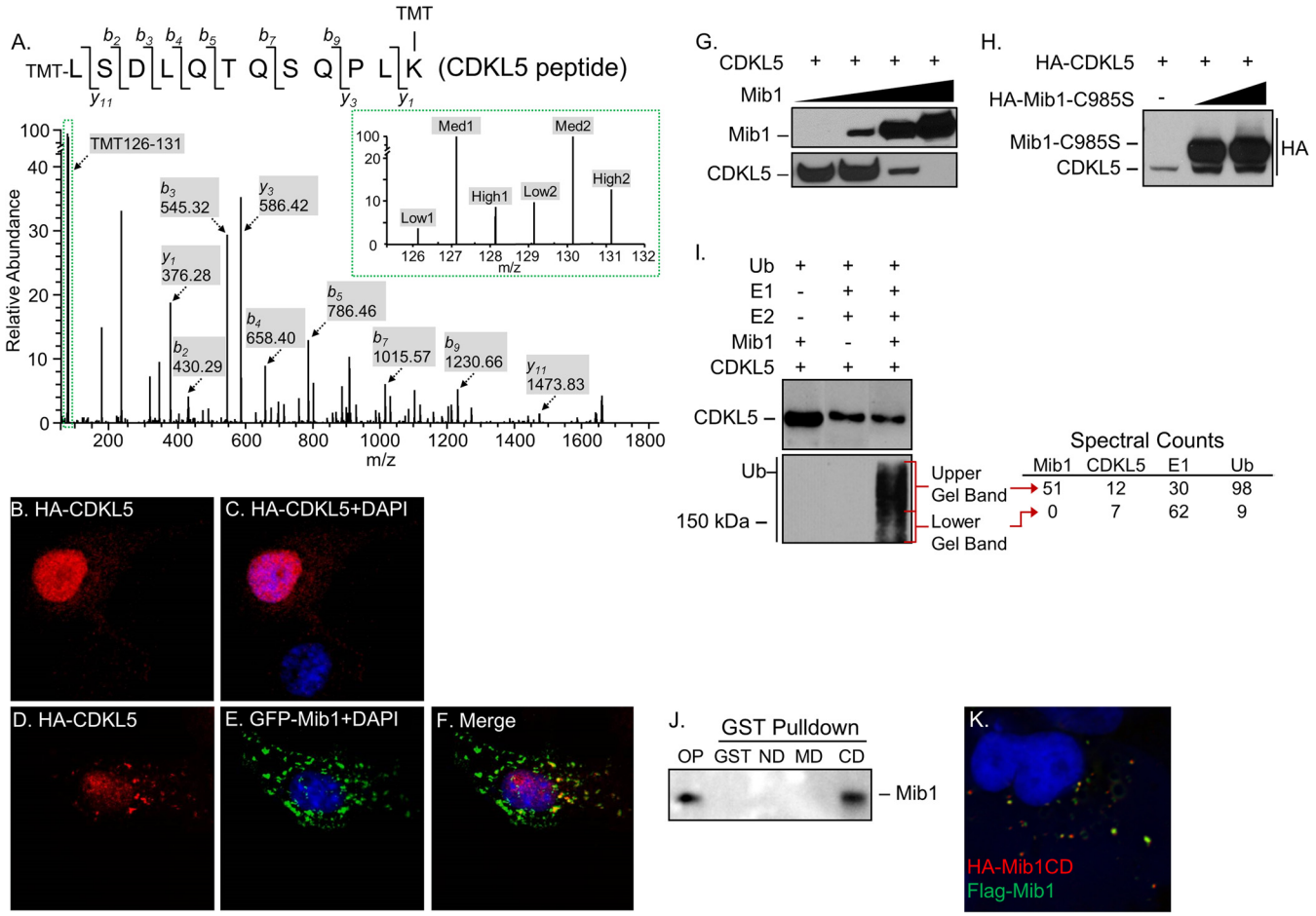

FIG. 6. **Mib1 colocalizes with and down-regulates CDKL5.** *A*, Representative MS2 spectrum depicting peptide 826–837 from CDKL5 protein and TMT reporter ion intensities (inset). *B–C*, Typical HA-CDKL5 localization in HEK293 cells is largely nuclear when expressed alone. *D–F*, Coexpression of HA-CDKL5 along with GFP-Mib1 led to redistribution of CDKL5 from the nucleus to puncta in cytoplasm. *G–H*, Western blot analysis of HA-CDLK5 and GFP-Mib1 cotransfected HEK293 cells, dependent on Mib1 ligase activity. C985S is a mutated form of Mib1 with abolished ligase activity. *I*, Western blot and LC-MS/MS analysis of ubiquitination of CDLK5 by Mib1. *J–K*, Western blot and immunofluorescence staining analysis show self-association of Mib1 through its C-terminal domain.

The synaptic Mib1 binding partners revealed in our study included the Ca^{2+}/calmodulin-dependent kinase family (Camk2b, d, and g), the Neurexin family (Nrxn1, 2, and 3), and the Signal-induced proliferation-associated 1 like family (Sipa1l1, 2, and 3). These span functions from dendritic spine morphology (63), plasticity at glutamatergic synapses (64), and structural connection at the synaptic cleft (65). These functions are not unlike the known Mib1 functional roles: structural changes through cytoskeletal remodeling and cell-to-cell connections, suggesting that Mib1 is a central agent to bridge these processes. Indeed there is significant overlap between synaptic modulators and proteins that promote cellular and neuronal morphogenesis. Proteins regulating morphogenic activity were even more strongly enriched in our data than synaptic proteins, supporting the role of Mib1 in regulating neurite outgrowth (12), cell polarity (60), and synaptic plasticity (11). Moreover, our data show Mib1 suppresses dendritic spine outgrowth and acts as an opposing force to CDKL5 and its spine outgrowth and maturation effects.

Regulation of CDKL5 by Mib1 suggests Mib1 controls multiple stages of neuronal and synaptic morphogenesis. CDKL5 has been shown to promote neuronal survival (66), neurite outgrowth (49), dendritic spine formation (50, 51), and is an excellent example of a Mib1 interaction partner that regulates both cytoskeleton morphology and synaptic activity—bridging these two interrelated processes. Mutations in CDKL5 cause extreme variants of Rett Syndrome (67), and EIEE2 (68) which are severe and progressive forms of mental retardation. Our experiments show that when Mib1 is in abundance relative to CDKL5, dendritic spine outgrowth is impaired. This may be an important consequence of the mutations seen in CDKL5-associated diseases. Removal of CDKL5 via deletions or mutations resulting in a nonfunctional protein may tip the balance away from signaling pathways that lead to cytoskeletal outgrowth and neuronal maturation, resigning developing

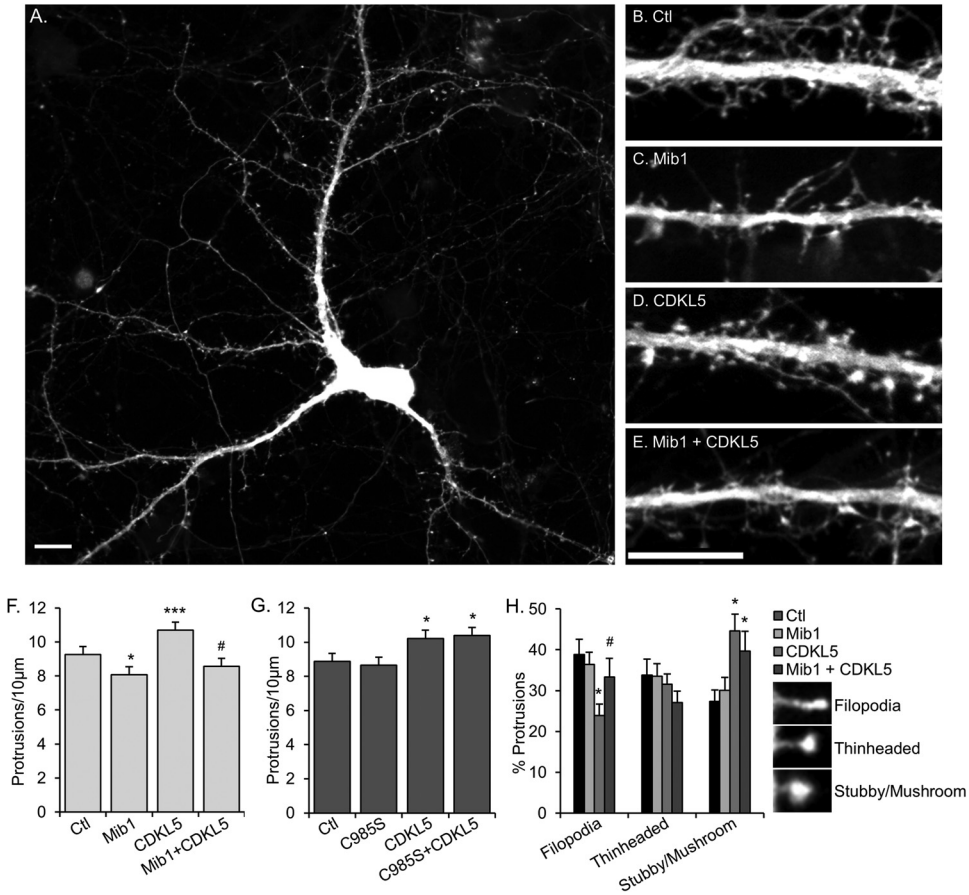

FIG. 7. **Mib1 inhibits dendritic spine outgrowth and limits pro-outgrowth effects of CDKL5 in neuronal culture.** *A*, Representative rat hippocampal neuron transfected at DIV7 with EGFP and stained for EGFP at DIV14. *B–E*, Higher magnification representative images of dendritic spines in control (Ctl, GFP only), Mib1, CDKL5, and Mib1 + CDKL5 transfected neurons, showing decreased outgrowth phenotype with Mib1 and Mib1 + CDKL5, and increased with CDKL5 and C985S + CDKL5. *F–G*, Quantitative analysis of dendritic spine density from these neurons. Analysis of the spine density showing mean ± S.E. per 10 μm, $n = 12$ for Ctl, $n = 16$ for Mib1, $n = 14$ for CDKL5, $n = 11$ for Mib1 + CDKL5 in experiment one; $n = 11$ for Ctl, $n = 34$ for C985S, $n = 27$ for CDKL5, $n = 12$ for C985S + CDKL5 in experiment two (* $p \leq 0.05$ from Ctl, *** $p \leq 0.001$ from Ctl, # $p \leq 0.05$ from CDKL5, *t* test). *H*, Classification and analysis of dendritic spine shapes in these neurons. Shape proportion analysis of the same neurons delineated between filopodia-, thinheaded-, and stubby/mushroom-shaped protrusions order of maturation. * $p \leq 0.05$ from Ctl, # $p \leq 0.05$ from CDKL5, *t* test). Scale bars, 10 μm.

neurons to an outcome with shorter processes and fewer synapses.

In summary, using our novel and widely applicable improvement to affinity purification proteomics, we uncovered the most comprehensive view of the Mib1 interactome to date and partitioned it by binding strength and confidence of interaction. Our experimental design utilized several recent advances in MS-based proteomics, TMT isobaric tags, and high resolution/high sensitivity mass spectrometry to attain this deep and distinguishing analysis. Our data reinforce the pivotal role of Mib1 in neuronal development and identify a large number of novel interaction partners. These interaction partners spread across such varied and critical signaling networks suggesting Mib1 may act as a hub to link these networks and perform a widely powerful governing role for cell, tissue, and organ development. Further work on this critical protein is certainly warranted as interactions with many well- and lesser-known molecules are highly likely to have functional ramifications.

Acknowledgments—We thank Christina Nemeth, Randy Watson, and members of the Enemark and Peng laboratories for helpful support and discussion during this study We have declared no conflicts of interest.

* This work was partially supported by NIH grant NS081571 and ALSAC (American Lebanese Syrian Associated Charities). The MS analysis was performed in the St. Jude Children's Research Hospital Proteomics Facility, partially supported by NIH Cancer Center Support Grant (P30CA021765). Imaging data were acquired at the Cell & Tissue Imaging Center which is supported by SJCRH and NCI P30 CA021765.

S This article contains supplemental Figs. S1 to S5 and Tables S1 and S2.

‖ To whom correspondence should be addressed: St. Jude Children's Research Hospital, MS311, D1034C 262 Danny Thomas Place, Memphis, TN 38105. Tel.: 901-595-7499; Fax: 901-595-3032; E-mail: junmin.peng@stjude.org.

REFERENCES

1. Itoh, M., Kim, C.-H., Palardy, G., Oda, T., Jiang, Y.-J., Maust, D., Yeo, S.-Y., Lorick, K., Wright, G. J., Ariza-McNaughton, L., Weissman, A. M., Lewis, J., Chandrasekharappa, S. C., and Chitnis, A. B. (2003) Mind bomb is a ubiquitin ligase that is essential for efficient activation of Notch signaling by Delta. *Dev. Cell* **4,** 67–82
2. Van Eeden, F. J., Granato, M., Schach, U., Brand, M., Furutani-Seiki, M., Haffter, P., Hammerschmidt, M., Heisenberg, C. P., Jiang, Y. J., Kane, D. A., Kelsh, R. N., Mullins, M. C., Odenthal, J., Warga, R. M., Allende, M. L., Weinberg, E. S., and Nüsslein-Volhard, C. (1996) Mutations affecting somite formation and patterning in the zebrafish, Danio rerio. *Development* **123,** 153–164
3. Haddon, C., Jiang, Y. J., Smithers, L., and Lewis, J. (1998) Delta-Notch signaling and the patterning of sensory cell differentiation in the zebrafish ear: evidence from the mind bomb mutant. *Development* **125,** 4637–4644
4. Lawson, N. D., Scheer, N., Pham, V. N., Kim, C. H., Chitnis, A. B., Campos-Ortega, J. A., and Weinstein, B. M. (2001) Notch signaling is required for arterial-venous differentiation during embryonic vascular development. *Development* **128,** 3675–3683
5. Capoccia, B. J., Jin, R. U., Kong, Y., Peek, R. M. Jr., Fassan, M., Rugge, M., and Mills, J. C. (2013) The ubiquitin ligase Mindbomb 1 coordinates gastrointestinal secretory cell maturation. *J. Clin. Invest.* **123,** 23–27
6. Koo, B.-K., Yoon, M.-J., Yoon, K.-J., Im, S.-K., Kim, Y.-Y., Kim, C.-H., Suh, P.-G., Jan, Y. N., and Kong, Y.-Y. (2007) An obligatory role of mind bomb-1 in notch signaling of mammalian development. *PLoS One* **2,** e1221
7. Liu, L.-J., Liu, T.-T., Ran, Y., Li, Y., Zhang, X.-D., Shu, H.-B., and Wang, Y.-Y. (2012) The E3 ubiquitin ligase MIB1 negatively regulates basal IκBα level and modulates NF-κB activation. *Cell Res.* **22,** 603–606
8. Altschul, S. F., Madden, T. L., Schäffer, A. A., Zhang, J., Zhang, Z., Miller, W., and Lipman, D. J. (1997) Gapped BLAST and PSI-BLAST: a new generation of protein database search programs. *Nucleic Acids Res.* **25,** 3389–3402
9. Takeuchi, T., Heng, H. H., Ye, C. J., Liang, S.-B., Iwata, J., Sonobe, H., and Ohtsuki, Y. (2003) Down-regulation of a novel actin-binding molecule, skeletrophin, in malignant melanoma. *Am. J. Pathol.* **163,** 1395–1404
10. Koo, B.-K., Lim, H.-S., Song, R., Yoon, M.-J., Yoon, K.-J., Moon, J.-S., Kim, Y.-W., Kwon, M.-C., Yoo, K.-W., Kong, M.-P., Lee, J., Chitnis, A. B., Kim, C.-H., and Kong, Y.-Y. (2005) Mind bomb 1 is essential for generating functional Notch ligands to activate Notch. *Development* **132,** 3459–3470
11. Yoon, K.-J., Lee, H.-R., Jo, Y. S., An, K., Jung, S.-Y., Jeong, M.-W., Kwon, S.-K., Kim, N.-S., Jeong, H.-W., Ahn, S.-H., Kim, K.-T., Lee, K., Kim, E., Kim, J.-H., Choi, J.-S., Kaang, B.-K., and Kong, Y.-Y. (2012) Mind bomb-1 is an essential modulator of long-term memory and synaptic plasticity via the Notch signaling pathway. *Mol. Brain* **5,** 40
12. Choe, E.-A., Liao, L., Zhou, J.-Y., Cheng, D., Duong, D. M., Jin, P., Tsai, L.-H., and Peng, J. (2007) Neuronal morphogenesis is regulated by the interplay between cyclin-dependent kinase 5 and the ubiquitin ligase mind bomb 1. *J. Neurosci.* **27,** 9503–9512
13. Tessier-Lavigne, M., and Goodman, C. S. (1996) The molecular biology of axon guidance. *Science* **274,** 1123–1133
14. Cline, H. T. (2001) Dendritic arbor development and synaptogenesis. *Curr. Opin. Neurobiol.* **11,** 118–126
15. Nimchinsky, E. a, Sabatini, B. L., and Svoboda, K. (2002) Structure and function of dendritic spines. *Annu. Rev. Physiol.* **64,** 313–353
16. Scheiffele, P. (2003) Cell–cell signaling during synapse formation in the CNS. *Annu. Rev. Neurosci.* **26,** 485–508
17. Kwon, D. Y., Dimitriadi, M., Terzic, B., Cable, C., Hart, A. C., Chitnis, A., Fischbeck, K. H., and Burnett, B. G. (2013) The E3 ubiquitin ligase mind bomb 1 ubiquitinates and promotes the degradation of survival of motor neuron protein. *Mol. Biol. Cell* **24,** 1863–1871
18. Berndt, J. D., Aoyagi, A., Yang, P., Anastas, J. N., Tang, L., and Moon, R. T. (2011) Mindbomb 1, an E3 ubiquitin ligase, forms a complex with RYK to activate Wnt/{beta}-catenin signaling. *J. Cell Biol.* **194,** 737–750
19. Tseng, L.-C., Zhang, C., Cheng, C.-M., Xu, H., Hsu, C.-H., and Jiang, Y.-J. (2014) New classes of mind bomb-interacting proteins identified from yeast two-hybrid screens. *PLoS One* **9,** e93394
20. Mann, M., Kulak, N. A., Nagaraj, N., and Cox, J. (2013) The coming age of complete, accurate, and ubiquitous proteomes. *Mol. Cell* **49,** 583–590
21. Zhang, Y., Fonslow, B. R., Shan, B., Baek, M., and Yates, J. R. (2013) Protein Analysis by Shotgun/Bottom-up Proteomics. *Chem. Rev.* **113,** 2343–2394
22. Gstaiger, M., and Aebersold, R. (2009) Applying mass spectrometry-based proteomics to genetics, genomics, and network biology. *Nat. Rev. Genet.* **10,** 617–627
23. Nesvizhskii, A. I. (2012) Computational and informatics strategies for identification of specific protein interaction partners in affinity purification mass spectrometry experiments. *Proteomics* **12,** 1639–1655
24. Rigaut, G., Shevchenko, A., Rutz, B., Wilm, M., Mann, M., and Séraphin, B. (1999) A generic protein purification method for protein complex characterization and proteome exploration. *Nat. Biotechnol.* **17,** 7–9
25. Guerrero, C., Tagwerker, C., Kaiser, P., and Huang, L. (2006) An integrated mass spectrometry-based proteomic approach: quantitative analysis of tandem affinity-purified *in vivo* cross-linked protein complexes (QTAX) to decipher the 26 S proteasome-interacting network. *Mol. Cell. Proteomics* **5,** 366–378
26. Kaake, R. M., Wang, X., and Huang, L. (2010) Profiling of protein interaction networks of protein complexes using affinity purification and quantitative mass spectrometry. *Mol. Cell. Proteomics* **9,** 1650–1665
27. Dayon, L., Hainard, A., Licker, V., Turck, N., Kuhn, K., Hochstrasser, D. F., Burkhard, P. R., and Sanchez, J.-C. (2008) Relative quantification of proteins in human cerebrospinal fluids by MS/MS using 6-plex isobaric tags. *Anal. Chem.* **80,** 2921–2931
28. Valli, E., Trazzi, S., Fuchs, C., Erriquez, D., Bartesaghi, R., Perini, G., and Ciani, E. (2012) CDKL5, a novel MYCN-repressed gene, blocks cell cycle, and promotes differentiation of neuronal cells. *Biochim. Biophys. Acta* **1819,** 1173–1185
29. Xu, P., Duong, D. M., and Peng, J. (2009) Systematical optimization of reverse-phase chromatography for shotgun proteomics research articles. *J. Proteome Res.* **8,** 3944–3950
30. Wang, H., Yang, Y., Li, Y., Bai, B., Wang, X., Tan, H., Liu, T., Beach, T. G., Peng, J., and Wu, Z. (2015) Systematic optimization of long gradient chromatography mass spectrometry for deep analysis of brain proteome. *J. Proteome Res.* **14,** 829–838
31. Peng, J., Elias, J. E., Thoreen, C. C., Licklider, L. J., and Gygi, S. P. (2003) Evaluation of multidimensional chromatography coupled with tandem mass spectrometry (LC/LC-MS/MS) for large-scale protein analysis: the yeast proteome. *J. Proteome Res.* **2,** 43–50
32. Peng, J., Schwartz, D., Elias, J. E., Thoreen, C. C., Cheng, D., Marsischky, G., Roelofs, J., Finley, D., and Gygi, S. P. (2003) A proteomics approach to understanding protein ubiquitination. *Nat. Biotechnol.* **21,** 921–926
33. Wang, X., Li, Y., Wu, Z., Wang, H., Tan, H., and Peng, J. (2014) JUMP: a tag-based database search tool for peptide identification with high sensitivity and accuracy. *Mol. Cell. Proteomics* **13,** 3663–3673
34. Wixon, J., and Kell, D. (2000) The Kyoto encyclopedia of genes and genomes–KEGG. *Yeast* **17,** 48–55
35. Huang, D. W., Sherman, B. T., and Lempicki, R. A. (2009) Systematic and integrative analysis of large gene lists using DAVID bioinformatics resources. *Nat. Protoc.* **4,** 44–57
36. Huang, D. W., Sherman, B. T., and Lempicki, R. A. (2009) Bioinformatics enrichment tools: paths toward the comprehensive functional analysis of large gene lists. *Nucleic Acids Res.* **37,** 1–13
37. Jensen, L. J., Kuhn, M., Stark, M., Chaffron, S., Creevey, C., Muller, J., Doerks, T., Julien, P., Roth, A., Simonovic, M., Bork, P., and von Mering, C. (2009) STRING 8–a global view on proteins and their functional interactions in 630 organisms. *Nucleic Acids Res.* **37,** D412–D416
38. Bai, B., Chen, P., Hales, C. M., Wu, Z., Pagala, V., High, A. A., Levey, A. I., Lah, J. J., and Peng, J. (2014) Integrated approaches for analyzing U1–70K cleavage in Alzheimer's disease. *J. Proteome Res.* **13,** 4526–4534
39. Terabayashi, T., Funato, Y., Fukuda, M., and Miki, H. (2009) A coated vesicle-associated kinase of 104 kDa (CVAK104) induces lysosomal degradation of frizzled 5 (Fzd5). *J. Biol. Chem.* **284,** 26716–26724
40. Brittain, J. M., Wang, Y., Wilson, S. M., and Khanna, R. (2012) Regulation of CREB signaling through L-type Ca2+channels by Nipsnap-2. *Channels* **6,** 94–102
41. Han, K.-J., Foster, D. G., Zhang, N.-Y., Kanisha, K., Dzieciatkowska, M., Sclafani, R. a, Hansen, K. C., Peng, J., and Liu, C.-W. (2012) Ubiquitin-specific protease 9x deubiquitinates and stabilizes the spinal muscular atrophy protein-survival motor neuron. *J. Biol. Chem.* **287,** 43741–43752

42. Homan, C. C., Kumar, R., Nguyen, L. S., Haan, E., Raymond, F. L., Abidi, F., Raynaud, M., Schwartz, C. E., Wood, S. a, Gecz, J., and Jolly, L. a (2014) Mutations in USP9X are associated with X-linked intellectual disability and disrupt neuronal cell migration and growth. *Am. J. Hum. Genet.* **94,** 470–478
43. Li, Y., Cheng, Y., Huang, Y., Conti, M., Wilson, S. P., Donnell, M. O., and Zhang, H. (2011) Phosphodiesterase-4D knockout and RNAi-mediated knockdown enhance memory and increase hippocampal neurogenesis via increased cAMP signaling. *J. Neurosci.* **31,** 172–183
44. Ethell, I. M., and Pasquale, E. B. (2005) Molecular mechanisms of dendritic spine development and remodeling. *Prog. Neurobiol.* **75,** 161–205
45. Stegeman, S., Jolly, L. A., Premarathne, S., Gecz, J., Richards, L. J., Mackay-Sim, A., and Wood, S. a (2013) Loss of Usp9x disrupts cortical architecture, hippocampal development, and TGFβ-mediated axonogenesis. *PLoS One* **8,** e68287
46. McCrea, P. D., and Gu, D. (2010) The catenin family at a glance. *J. Cell Sci.* **123,** 637–642
47. Wang, I.-T. J., Allen, M., Goffin, D., Zhu, X., Fairless, A. H., Brodkin, E. S., Siegel, S. J., Marsh, E. D., Blendy, J. a, and Zhou, Z. (2012) Loss of CDKL5 disrupts kinome profile and event-related potentials leading to autistic-like phenotypes in mice. *Proc. Natl. Acad. Sci. U.S.A.* **109,** 21516–21521
48. Tavyev Asher, Y. J., and Scaglia, F. (2012) Molecular bases and clinical spectrum of early infantile epileptic encephalopathies. *Eur. J. Med. Genet.* **55,** 299–306
49. Chen, Q., Zhu, Y.-C., Yu, J., Miao, S., Zheng, J., Xu, L., Zhou, Y., Li, D., Zhang, C., Tao, J., and Xiong, Z.-Q. (2010) CDKL5, a protein associated with rett syndrome, regulates neuronal morphogenesis via Rac1 signaling. *J. Neurosci.* **30,** 12777–12786
50. Ricciardi, S., Ungaro, F., Hambrock, M., Rademacher, N., Stefanelli, G., Brambilla, D., Sessa, A., Magagnotti, C., Bachi, A., Giarda, E., Verpelli, C., Kilstrup-Nielsen, C., Sala, C., Kalscheuer, V. M., and Broccoli, V. (2012) CDKL5 ensures excitatory synapse stability by reinforcing NGL-1-PSD95 interaction in the postsynaptic compartment and is impaired in patient iPSC-derived neurons. *Nat. Cell Biol.* **14,** 1–15
51. Zhu, Y.-C., Li, D., Wang, L., Lu, B., Zheng, J., Zhao, S.-L., Zeng, R., and Xiong, Z.-Q. (2013) Palmitoylation-dependent CDKL5-PSD-95 interaction regulates synaptic targeting of CDKL5 and dendritic spine development. *Proc. Natl. Acad. Sci.* **110,** 9118–9123
52. Teo, G., Liu, G., Zhang, J., Nesvizhskii, A. I., Gingras, A.-C., and Choi, H. (2014) SAINTexpress: improvements and additional features in Significance Analysis of INTeractome software. *J. Proteomics* **100,** 37–43
53. Rüdiger, A. H., Rüdiger, M., Carl, U. D., Chakraborty, T., Roepstorff, P., and Wehland, J. (1999) Affinity mass spectrometry-based approaches for the analysis of protein-protein interaction and complex mixtures of peptide-ligands. *Anal. Biochem.* **275,** 162–170
54. Righetti, P. G. (2014) The Monkey King: A personal view of the long journey towards a proteomic Nirvana. *J. Proteomics* **107,** 39–49
55. Song, R., Koo, B.-K., Yoon, K.-J., Yoon, M.-J., Yoo, K.-W., Kim, H.-T., Oh, H.-J., Kim, Y.-Y., Han, J.-K., Kim, C.-H., and Kong, Y.-Y. (2006) Neuralized-2 regulates a Notch ligand in cooperation with Mind bomb-1. *J. Biol. Chem.* **281,** 36391–36400
56. Barsi, J. C., Rajendra, R., Wu, J. I., and Artzt, K. (2005) Mind bomb1 is a ubiquitin ligase essential for mouse embryonic development and Notch signaling. *Mech. Dev.* **122,** 1106–1117
57. Yoon, K.-J., Koo, B.-K., Im, S.-K., Jeong, H.-W., Ghim, J., Kwon, M.-C., Moon, J.-S., Miyata, T., and Kong, Y.-Y. (2008) Mind bomb 1-expressing intermediate progenitors generate notch signaling to maintain radial glial cells. *Neuron* **58,** 519–531
58. Yamamoto, M., Morita, R., Mizoguchi, T., Matsuo, H., Isoda, M., Ishitani, T., Chitnis, A. B., Matsumoto, K., Crump, J. G., Hozumi, K., Yonemura, S., Kawakami, K., and Itoh, M. (2010) Mib-Jag1-Notch signaling regulates patterning and structural roles of the notochord by controlling cell-fate decisions. *Development* **137,** 2527–2537
59. Daskalaki, A., Shalaby, N. A., Kux, K., Tsoumpekos, G., Tsibidis, G. D., Muskavitch, M. A. T., and Delidakis, C. (2011) Distinct intracellular motifs of Delta mediate its ubiquitylation and activation by Mindbomb1 and Neuralized. *J. Cell Biol.* **195,** 1017–1031
60. Dong, Z., Yang, N., Yeo, S.-Y., Chitnis, A., and Guo, S. (2012) Intralineage directional Notch signaling regulates self-renewal and differentiation of asymmetrically dividing radial glia. *Neuron* **74,** 65–78
61. Meloty-Kapella, L., Shergill, B., Kuon, J., Botvinick, E., and Weinmaster, G. (2012) Notch ligand endocytosis generates mechanical pulling force dependent on dynamin, epsins, and actin. *Dev. Cell* **22,** 1299–1312
62. Blitzer, J. T., and Nusse, R. (2006) A critical role for endocytosis in Wnt signaling. *BMC Cell Biol.* **7,** 28
63. Pak, D. T., Yang, S., Rudolph-Correia, S., Kim, E., and Sheng, M. (2001) Regulation of dendritic spine morphology by SPAR, a PSD-95-associated RapGAP. *Neuron* **31,** 289–303
64. Borgesius, N. Z., van Woerden, G. M., Buitendijk, G. H. S., Keijzer, N., Jaarsma, D., Hoogenraad, C. C., and Elgersma, Y. (2011) βCaMKII plays a nonenzymatic role in hippocampal synaptic plasticity and learning by targeting αCaMKII to synapses. *J. Neurosci.* **31,** 10141–10148
65. Südhof, T. C. (2008) Neuroligins and neurexins link synaptic function to cognitive disease. *Nature* **455,** 903–911
66. Fuchs, C., Trazzi, S., Torricella, R., Viggiano, R., De Franceschi, M., Amendola, E., Gross, C., Calzà, L., Bartesaghi, R., and Ciani, E. (2014) Loss of CDKL5 impairs survival and dendritic growth of newborn neurons by altering AKT/GSK-3β signaling. *Neurobiol. Dis.* **70,** 53–68
67. Artuso, R., Mencarelli, M. A., Polli, R., Sartori, S., Ariani, F., Pollazzon, M., Marozza, A., Cilio, M. R., Specchio, N., Vigevano, F., Vecchi, M., Boniver, C., Dalla Bernardina, B., Parmeggiani, A., Buoni, S., Hayek, G., Mari, F., Renieri, A., and Murgia, A. (2010) Early-onset seizure variant of Rett syndrome: definition of the clinical diagnostic criteria. *Brain Dev.* **32,** 17–24
68. Fehr, S., Wilson, M., Downs, J., Williams, S., Murgia, A., Sartori, S., Vecchi, M., Ho, G., Polli, R., Psoni, S., Bao, X., de Klerk, N., Leonard, H., and Christodoulou, J. (2013) The CDKL5 disorder is an independent clinical entity associated with early-onset encephalopathy. *Eur. J. Hum. Genet.* **21,** 266–273